NANO LETTERS

Letter

pubs.acs.org/NanoLett

All-Electrical Measurement of Interfacial Dzyaloshinskii-Moriya Interaction Using Collective Spin-Wave Dynamics

Jong Min Lee,[†] Chaun Jang,[†] Byoung-Chul Min,*[,†] Seo-Won Lee,[‡] Kyung-Jin Lee,[‡] and Joonyeon Chang[†]

[†]Center for Spintronics, Korea Institute of Science and Technology, Seoul 136-791, Korea

[‡]Department of Materials Science and Engineering and KU-KIST Graduate School of Converging Science and Technology, Korea University, Seoul 136-701, Korea

Supporting Information

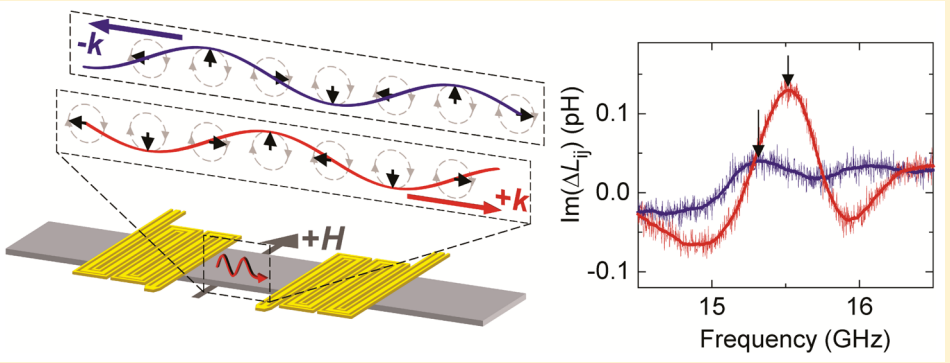

ABSTRACT: Dzyaloshinskii-Moriya interaction (DMI), which arises from the broken inversion symmetry and spin−orbit coupling, is of prime interest as it leads to a stabilization of chiral magnetic order and provides an efficient manipulation of magnetic nanostructures. Here, we report all-electrical measurement of DMI using propagating spin wave spectroscopy based on the collective spin wave with a well-defined wave vector. We observe a substantial frequency shift of spin waves depending on the spin chirality in Pt/Co/MgO structures. After subtracting the contribution from other sources to the frequency shift, it is possible to quantify the DMI energy in Pt/Co/MgO systems. The result reveals that the DMI in Pt/Co/MgO originates from the interfaces, and the sign of DMI corresponds to the inversion asymmetry of the film structures. The electrical excitation and detection of spin waves and the influence of interfacial DMI on the collective spin-wave dynamics will pave the way to the emerging field of spin-wave logic devices.

KEYWORDS: *Dzyaloshinskii-Moriya interaction, spin wave, magnetic thin film, chiral magnet, propagating spin wave spectroscopy, spintronics*

The Heisenberg exchange interaction, symmetric with respect to the inversion of a system, gives rise to a magnetic order in ferromagnetic materials. When the inversion symmetry is broken in a ferromagnetic system with strong spin−orbit coupling, there exists a non-negligible antisymmetric exchange interaction, namely Dzyaloshinskii-Moriya interaction (DMI).[1,2] The Hamiltonian of DMI between two adjacent atomic spins S_i and S_j is described as

$$H_{DMI} = -\mathbf{D}_{ij}\cdot(S_i \times S_j) \quad (1)$$

where $\mathbf{D}_{ij}$ is the DM vector, which is perpendicular to both the axis of broken symmetry and the distance vector connecting two spins.[2] The presence of DMI in a magnetic system favors noncollinear spin alignment and leads to chiral spin textures.[3−5] The DMI is observed not only in bulk materials (e.g., B20 materials such as MnSi and FeGe)[4,5] but also in magnetic nanostructures[6] where the inversion symmetry is broken at the interfaces with strong spin−orbit coupling. The interfacial DMI (i-DMI) plays a key role in magnetic dynamics in ferromagnetic nanostructures.[7−13] In order to understand the effect of i-DMI in such systems, it is important to measure the sign and magnitude of i-DMI,[11−13] which can be determined by investigating how the energy of a magnetic system changes with chirality inversion.

Spin wave provides a unique tool to study the DMI. The influence of DMI on the spin-wave dispersion has been predicted theoretically[14] and measured experimentally in an Fe double layer grown on W(110).[15] Recently, Cortés-Ortuño and Landeros[16] reported the DMI effect on the spin wave dispersion for various crystal symmetries, and Moon et al.[17] showed that by comparing the analytical equation with micromagnetic simulation the asymmetric spin wave propagation in a ferromagnetic/nonmagnet bilayer provides an access to a quantitative measurement of i-DMI energy. These

Received: July 9, 2015
Revised: November 14, 2015
Published: December 14, 2015

DOI: 10.1021/acs.nanolett.5b02732
Nano Lett. 2016, 16, 62−67

theoretical studies motivate several experimental works to quantify i-DMI in such magnetic nanostructures using the Brillouin light spectroscopy (BLS).[18−22]

Here we use an all-electrical method, propagating spin wave spectroscopy (PSWS),[23] based on the spin wave propagation with a well-defined spin wave vector. The resolution of spin wave vector is determined by antenna design. This all-electrical method allows us to determine the sign and magnitude of i-DMI covering a wide range of ferromagnetic structures. If there is a very thick heavy-metal layer on top of a magnetic layer or a capping layer with very rough surface, it is difficult to use BLS to measure the spin wave. By contrast, this electrical method can be used to measure the DMI of magnetic layers buried under a thick metallic capping layer such as in substrate/oxide/ferromagnet/heavy metal structures. This method is relatively free from possible artifacts caused by nonlinear interaction of thermal magnons having various wave vectors, which might be critical for the BLS investigation. In addition, our electrical approach raises prospects to design a new class of spintronic devices based on spin wave and i-DMI.

In the magnetostatic surface wave (MSSW) or Damon-Eshbach (DE) mode,[24] where the magnetization polarity ($p = \pm 1$) is perpendicular to the spin wave vector (k), the k and p determines the spatial chirality of spin alignment (Figure 1). This is because, given the propagation direction, the direction of magnetization determines the orientation of spin precession and thereby the spin chirality. For instance, when the magnetization is along the $+y$-axis, the spin wave propagating with wave vector $+k$ ($-k$) has a counterclockwise (clockwise) rotation of spins as shown in Figure 1a. The presence of i-DMI could lift the degeneracy in the spin wave frequency (f), resulting in asymmetric frequency response with respect to k.[16,17] The dispersion relation of the spin wave in the ferromagnet/nonmagnet bilayer system with i-DMI is given by

$$f = \frac{\gamma}{2\pi}\left[\sqrt{(H + 4\pi M_s P_k)(H - H_A + 4\pi M_s(1 - P_k))} + \frac{2pDk}{M_s}\right] \quad (2)$$

where γ is the gyromagnetic ratio, H is the external magnetic field, M_s is the saturation magnetization, P_k is the dynamic dipole field factor,[25] $P_k = 1 - (1 - \exp(-|k|t))/|k|t$, and H_A ($= H_{A,top} + H_{A,bottom}$) is the anisotropy field on the top and bottom surfaces of ferromagnetic film, t is the thickness of ferromagnetic layer, and D is the effective magnitude of DMI energy per unit area averaged across the ferromagnetic layer.

In order to measure the effect of i-DMI on the spin wave frequency, we prepare ferromagnetic film structures consisting of substrate/Ta (3 nm)/Pt (3 nm)/Co (t nm)/MgO (1.8 nm)/Ta (3 nm), hereafter referred to as the Pt/Co (t)/MgO samples. The film stacks are grown on oxidized silicon substrates by magnetron sputtering and patterned into 8 μm wide strip; thereafter a 40 nm thick AlO_x layer is deposited on the strip for electrical insulation. On top of the ferromagnet (FM) strip and AlO_x insulation, a pair of meander-shaped antennae (Figure 1b) are formed by a lift-off of Ti (5 nm)/Au (150 nm). The spatial period of the meander lines determines the k of spin wave (see Supporting Information Note 1). During the measurement, a static magnetic field is applied in the transverse direction (y-direction) to secure the MSSW mode. The antenna connected to a microwave source generates spatially periodic magnetic field, which in turn excites spin waves in the FM strip with a well-defined k, and the second antenna located at the other end detects the propagated spin

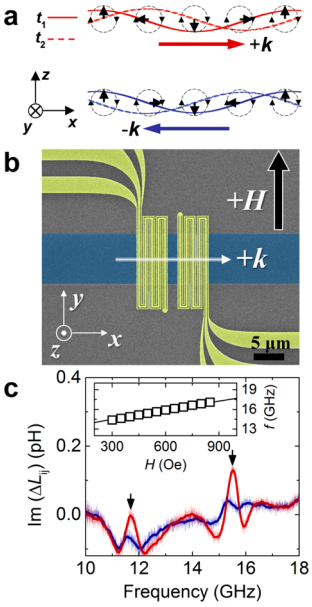

Figure 1. Spin configuration, the measurement geometry for propagating spin wave spectroscopy, and the frequency response of spin wave propagation. (a) Schematic diagram of counterclockwise (clockwise) spin alignment of the spin wave propagating with $+k$ ($-k$) taken at time t_1 and t_2 ($t_2 > t_1$). (b) Scanning electron micrograph image of the measurement geometry showing ferromagnet strip (blue) for the spin wave propagation in the longitudinal (x) direction and meander-line antennae (yellow) for the spin wave injection and detection. External magnetic field (H) is applied in the transverse (y) direction. (c) The imaginary part of mutual inductances, Im(ΔL_{ij}), of an Pt/Co (20)/MgO sample displaying an absorption of spin waves at the detecting antenna ($k = 7.85\ \mu m^{-1}$) as a consequence of spin wave resonance. The ΔL_{21} (red line) and ΔL_{12} (blue line) correspond, respectively, to the spin wave propagating in the forward (from the left to the right antenna) and the reverse (from the right to the left antenna) directions. Inset: The measured frequency of resonance peak (symbols) of the Pt/Co (20)/MgO sample with $k = 7.85\ \mu m^{-1}$ as a function of external magnetic field and the calculated frequency (line) using eq 2.

waves inductively. With interchanging the injector and detector antenna, we can manipulate the propagating direction of the spin waves.

The imaginary part of mutual inductance, Im(ΔL_{ij}), displays an absorption of spin waves at the detecting antenna as a consequence of spin wave resonance (see Methods). Figure 1c shows an example of the measured Im(ΔL_{ij}) of an Pt/Co (20)/MgO sample when the spatial period of antenna is 800 nm ($k = 7.85\ \mu m^{-1}$) and the applied transverse field (H) is +500 Oe. The ΔL_{21} (red line) and ΔL_{12} (blue line) correspond, respectively, to the spin wave propagating in the forward (from the left to the right antenna) and the reverse (from the right to the left antenna) directions. The antenna with the meander-pattern excites spin waves at two different frequencies (see Supporting Information Note 1); for instance, the main peak of Im(ΔL_{21}) at 15.5 GHz (red line) corresponds to the primary spatial period of the meander antenna (800 nm, $k_M = 7.85\ \mu m^{-1}$), and the secondary peak at 11.7 GHz corresponds to the subsidiary spatial period of the antenna (2250 nm, $k_S = 2.8\ \mu m^{-1}$). The nonzero baseline in Figure 1c is attributed to the phase delay during spin wave propagation and the impedance change of the antennae as a function of external magnetic field.[26] The inset of Figure 1c shows the frequency of

DOI: 10.1021/acs.nanolett.5b02732
Nano Lett. 2016, 16, 62−67

the primary peak of the Pt/Co (20)/MgO sample with $k = 7.85$ μm^{-1} as a function of external magnetic field. The frequency of the primary peak increases with increasing the transverse field (inset of Figure 1c), and the MSSW dispersion relation with $\gamma = 1.77 \times 10^{-2}$ $Oe^{-1}{\cdot}ns^{-1}$, $M_s = 1430$ emu/cm^3, and $H_A = 770$ Oe gives a good fit to the data (M_s and H_A are measured by a vibrating sample magnetometer. See Supporting Information Note 2).

In the MSSW mode, the propagating spin wave is partially localized on either the top or bottom surface of ferromagnetic layer depending on the propagation direction.[24,27] The signal amplitude of the forward-going spin wave ($+k$) at the antenna could be significantly different from that of the reverse-going spin wave ($-k$); this is known as the nonreciprocal spin wave propagation typically observed in the PSWS.[28−32] The difference in the amplitude of the inductively measured signal (Figure 1c) arises from the combination of two origins; the first is the localization of propagating spin wave in the DE mode, and the second is the asymmetric distribution of the excitation field from the antennae and relative sensitivity of the antenna on the direction of spin-wave propagation.[30−32] When there is no contribution from the DMI and interfacial magnetic anisotropy, the resonance frequency should be the same for both directions. The most important feature in Figure 1c is therefore a clear asymmetry in the frequency response; the peaks in ΔL_{21} show higher resonance frequencies in comparison with the peaks in ΔL_{12}.

We check whether the asymmetry in the frequency response agrees with what has been predicted in the presence of i-DMI.[16,17] Figure 2 shows the zoomed-in frequency response of

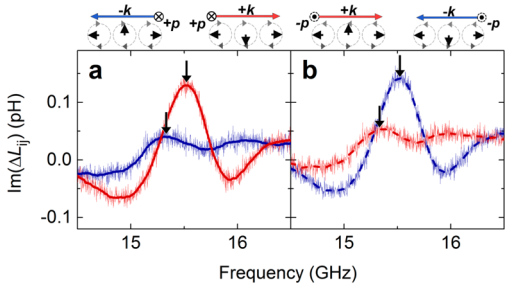

Figure 2. Asymmetric spin wave propagation in the Pt/Co(20)/MgO sample. The imaginary part of mutual inductances, Im(ΔL_{ij}), displaying the absorption of spin waves at the detecting antenna as a consequence of spin wave resonance ($k = 7.85$ μm^{-1} and $H = 500$ Oe). (a) Frequency response of spin wave with $-k$, $+p$ (blue solid line) and with $+k$, $+p$ (red solid line). (b) Frequency response of spin wave with $-k$, $-p$ (blue dashed line) and with $+k$, $-p$ (red dashed line). Schematic diagrams of spin alignment are shown for each combination of k and p.

the main peak with varying the propagation direction and polarity of the transverse field. When a positive transverse field ($H = +500$ Oe) is applied, the forward-going (reverse-going) spin wave has a counterclockwise (clockwise) spin chirality; the forward-going ($+k$) spin wave shows a signal maximum at 15.48 ± 0.01 GHz whereas the reverse-going ($-k$) spin wave shows a signal maximum at 15.32 ± 0.01 GHz. A substantial frequency difference ($\Delta f = f(+k) - f(-k) = +160$ MHz) between two maxima is observed with respect to the change of propagation direction. When the sign of transverse field (p) is reversed (Figure 2b), the forward-going spin wave ($+k$) shows a peak at a lower frequency in comparison with reverse-going spin wave ($-k$). The frequency difference ($\Delta f = f(+k) - f(-k) = -160$ MHz) in this case has the opposite sign, and the magnitude of Δf is the same as the previous case. Various combinations of k and p show that the counterclockwise chiral alignment results in a higher spin wave frequency than the clockwise alignment in this system. This is exactly what is predicted by the theory.[16,17]

An important question is how this frequency shift is related to i-DMI. A precise estimation of i-DMI requires a delicate consideration to distinguish the pure contribution of i-DMI from other sources such as the nonreciprocity of MSSW mode and the influence of interfacial magnetic anisotropy.[20] We should take into account that the propagating spin wave is partially localized on either the top or bottom interface of ferromagnetic layer depending on the propagation direction. Hence, if the top interface has a substantially different interface anisotropy in comparison with that of the bottom interface, this may result in a frequency shift (Δf_{ks}) with respect to the sign change of k or p (see Supporting Information Note 3). Therefore, the measured frequency difference (Δf) could be a sum of both the Δf_{DMI} from i-DMI and Δf_{ks} from the interfacial anisotropy difference.

A useful test to distinguish the pure contribution from i-DMI is to examine how the frequency shift is dependent on the wave vector (k) and the thickness of Co layer (t). In order to study the k and t dependence, we prepare four Pt/Co (t)/MgO samples by changing the k from 2.62 to 7.85 μm^{-1} with a fixed t of 20 nm and three samples by changing the t from 16 to 20 nm with a fixed k of 5.23 μm^{-1}. The measured frequency shift (Figure 3a,b) is increased monotonically with increasing k and $1/t$. In order to estimate the magnitude of i-DMI, the contribution of Δf_{ks} on the measured Δf is carefully subtracted. The interface anisotropy (K_i) on the Pt/Co interface is 1.1 erg/cm^2, and the K_i on the Co/MgO interface is negligible without

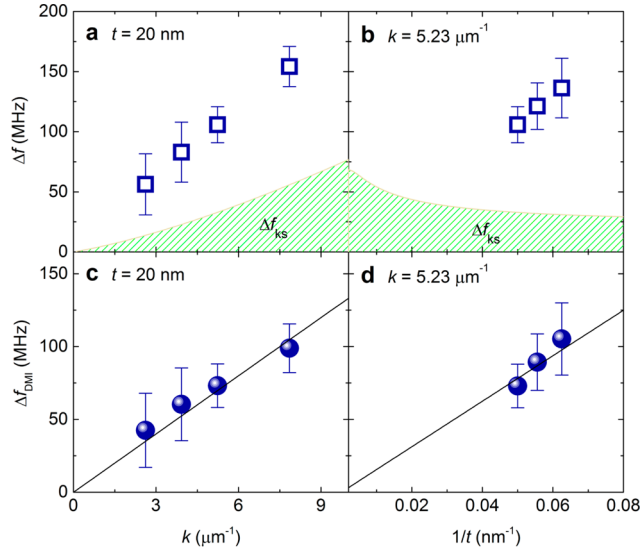

Figure 3. Frequency difference with respect to the change of spin chirality in the Pt/Co(t)/MgO samples. (a) Measured frequency difference (Δf) as a function of wave vector (k) with a fixed t of 20 nm. (b) Δf as a function of the reciprocal of Co film thickness ($1/t$) with a fixed k of 5.23 μm^{-1}. (c) Frequency difference originating from i-DMI (Δf_{DMI}) as a function of wave vector (k) with a fixed t of 20 nm. (d) Δf_{DMI} as a function of $1/t$ with a fixed k of 5.23 μm^{-1}. Error bars indicate the standard deviation of the several measurements with varying combination of k and p. Hatched region indicates the frequency shift induced by the interface anisotropy.

DOI: 10.1021/acs.nanolett.5b02732
Nano Lett. 2016, 16, 62−67

annealing (see Supporting Information Note 2). Using eq 2, we estimate the frequency shift arising from the interfacial anisotropy difference. The contribution of Δf_{ks}, which is not negligible, is shown as a hatched region in Figure 3a,b. Because the estimated Δf_{ks} also increases with increasing k, it is not conclusive to exclude the contribution of Δf_{ks} by comparing only the magnitude of Δf and Δf_{ks}. On the other hand, the thickness dependence of measured Δf sheds light on this matter. As we increase $1/t$ (or decrease the film thickness), the estimated Δf_{ks} is expected to decrease, but the measured Δf apparently increases (Figure 3b). This result demonstrates that the measured Δf cannot arise solely from the interface anisotropy difference, but the major part of Δf originates from the i-DMI. As shown in Figure 3c,d, the Δf_{DMI} from i-DMI is obtained by subtracting the Δf_{ks} from the measured Δf; approximately $\Delta f_{DMI} = \Delta f - \Delta f_{ks}$. The magnitude of i-DMI is then determined using[17]

$$D = \frac{\pi M_s}{2\gamma|k|}\Delta f_{DMI} \tag{3}$$

The measurement of DMI as a function of Co thickness provides important insights on the nature of the DMI in Pt/Co (t)/MgO structures. The top panel of Figure 4a shows the measured D of Pt/Co (t)/MgO samples. It is noteworthy that the D is proportional to $1/t$, displaying the interfacial origin of the DMI. We presume that, given the roughness of the Pt/Co interface, only a few monolayers at the interface with a characteristic length (λ) contribute to i-DMI. The measured D, the thickness average of i-DMI, can be expressed in terms of the magnitude of i-DMI (D_i) on the interface

$$D = \frac{D_i\lambda}{t} \tag{4}$$

It is possible that the $D_i\lambda$ is dependent on the detailed properties of the interface such as the roughness and texture of the Pt/Co film.[19] If the Pt/Co interface is abrupt and Co has an FCC structure, the λ is determined by the distance of closest approach (0.25 nm). Then the upper bound of D_i at the Pt/Co interface is estimated to be 14.7 ± 0.3 erg/cm^2. Simply assuming the $D_i\lambda$ remains constant as a function of t and using the measured D of Pt/Co (16 nm)/MgO, we estimate the D of Pt/Co (2 nm)/MgO is ∼1.8 erg/cm^2, which is comparable in magnitude to the previously reported results with a similar ferromagnet thickness.[9,18,19]

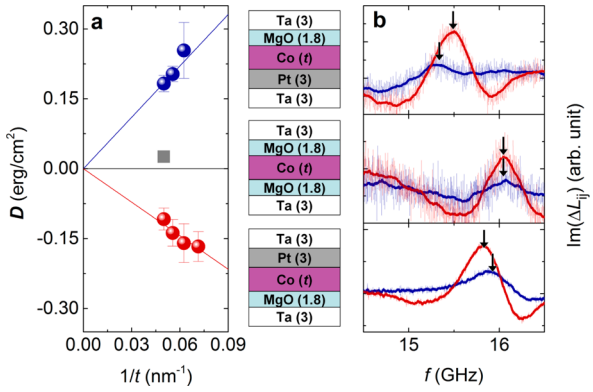

Figure 4. Interfacial DMI depending on the sample asymmetry and corresponding frequency response of spin wave propagation. (a) Measured DMI (D) of the MgO/Co (t nm)/Pt (red circles) and Pt/Co (t nm)/MgO (blue circles) samples as a function of the reciprocal of Co film thickness ($1/t$) with a fixed k of 7.85 μm^{-1}. The D of an MgO/Co/MgO sample having symmetric interfaces (square) is also shown. (b) The imaginary part of mutual inductances, Im(ΔL_{ij}), measured with Pt/Co (20 nm)/MgO (top panel), MgO/Co (20 nm)/MgO (center panel), and MgO/Co (20 nm)/Pt (bottom panel) samples. Corresponding sample structures are shown on the left of the panels. The frequency responses are obtained with k = +7.85 μm^{-1} (red lines) and k = −7.85 μm^{-1} (blue lines) with applying H = +500 Oe. The peak frequencies are indicated by arrows.

The sign of i-DMI is positive in the Pt/Co (t)/MgO samples, meaning that the clockwise spin alignment is energetically more stable than the counterclockwise spin alignment in this system. In order to investigate whether the sign of i-DMI corresponds to the inversion asymmetry of the film structures, we prepare inverted structures consisting of substrate/Ta (3 nm)/MgO (1.8 nm)/Co (t nm)/Pt (3 nm)/Ta (3 nm) referred to as MgO/Co (t)/Pt samples; and a symmetric structure consisting of substrate/Ta (3 nm)/MgO (1.8 nm)/Co (20 nm)/MgO (1.8 nm)/Ta (3 nm) referred to as an MgO/Co/MgO sample. Figure 4b shows the measured Im(ΔL_{ij}) of three different samples when a spatial period of antenna is 800 nm (k = 7.85 μm^{-1}) and a transverse field (H) is +500 Oe. The inverted MgO/Co/Pt samples (bottom panel) also show a substantial frequency shift, but the sign of frequency shift is now opposite to that of the Pt/Co/MgO structures (top panel). For the MgO/Co/Pt (Pt/Co/MgO) structures, the forward-going spin wave shows a peak at a lower (higher) frequency in comparison with that of the reverse-going spin wave, implying that the counterclockwise (clockwise) alignment is energetically more stable than the clockwise (counterclockwise) alignment in MgO/Co/Pt (Pt/Co/MgO) systems. This sign reversal of frequency shift once again strongly supports that the measured frequency shift is dominantly induced by i-DMI, because the DMI vector changes its sign with the structure inversion. It is noteworthy that the MgO/Co/MgO sample (center panel) having nominally symmetric interfaces shows a negligible frequency shift, implying that the contribution from the top Co/MgO interface has been canceled out by the contribution from the bottom MgO/Co interface. The difference in the interfacial anisotropy of the samples also results in the difference in spin wave resonance frequencies (see Supporting Information Note 4 for the details). In conclusion, the electrical measurement of i-DMI by collective spin wave dynamics shows that the DMI in Pt/Co/MgO originates from interfaces, and the sign of i-DMI corresponds to the inversion asymmetry of the film structures.

A remaining question is which interface, MgO/Co or Co/Pt, dominantly contributes to the measured DMI. The D of the inverted MgO/Co (t)/Pt samples is also proportional to $1/t$ (Figure 4a) but the slope ($D_i\lambda$) of MgO/Co (t)/Pt samples is not exactly the same as that of Pt/Co (t)/MgO samples. This indicates that the texture and roughness at the top Co/Pt interface is somehow different from those at the bottom Pt/Co interface. One can speculate that the i-DMI might dominantly originate from the Co/Pt or Pt/Co interface with strong spin orbit coupling than the MgO/Co or Co/MgO interface, but a systematic investigation is required to verify this conjecture. It has been reported that the magnetic ordering temperature of nonmagnetic/ferromagnet bilayer (e.g., W/Gd) is dependent on the ferromagnet thickness.[33] We expect similar thickness dependence of ferromagnetic ordering in the Co/Pt bilayers, and a strong DMI may contribute to this weak ferromagnetim at the interface. The effective thickness of Co layer (t*) is

DOI: 10.1021/acs.nanolett.5b02732
Nano Lett. 2016, 16, 62−67

determined from a linear fit of $M_s t$ versus t data (t is the deposited Co thickness). The effective Co thicknesses (t^*) of the Pt/Co/MgO, MgO/Co/Pt and MgO/Co/MgO are $t - 0.64 \pm 0.01$ nm, $t - 0.14 \pm 0.05$ nm and $t - 0.00 \pm 0.17$ nm, respectively. It should be noted that the effective thickness of Co layer (t^*) is smaller than the deposited Co thickness (t) in the Pt/Co/MgO and MgO/Co/Pt samples. This indicates that the reduction of ferromagnetic magnetic ordering occurs mainly at the Pt/Co or Co/Pt interface. Recent theoretical studies showed that the DMI at Co layers away from the Co/Pt interface is not negligible and a considerable i-DMI exists even when the Co and Pt atoms are intermixed.[34,35]

The all-electrical approach using the collective spin wave dynamics can be applied not only to measure i-DMI energy in various ferromagnetic systems but also to design novel spin-wave logic devices.[32,36−38] For instance, if the i-DMI or interfacial anisotropy is controlled by applying external voltage,[37,39] a sort of spin wave modulators can be realized as depicted in Figure 5a. This spin-wave modulator has a gate for

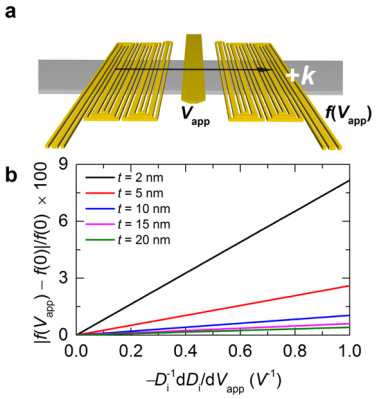

Figure 5. Frequency modulation of spin wave by voltage bias. (a) Schematic diagram of a spin-wave modulator with an external voltage bias, which is assumed to control the magnitude of interfacial DMI (D_i). The spin-wave frequency ($f(V_{app})$) at the detector is calculated as a function of voltage bias (V_{app}) using eq 2 with following parameters: H = +200 Oe, M_s = 1430 emu/cm^3, D_i (0 V)= 14.7 erg/cm^2. (b) Calculated frequency modulation as a function of dD_i/dV_{app}.

the external voltage bias, which is assumed to change the magnitude of interfacial DMI (D_i). Considering the influence of D_i in eq 2, we can calculate the frequency of propagating spin wave as a function of voltage bias (V_{app}). Figure 5b shows the calculated results for the frequency modulation as a function of dD_i/dV_{app}. It turns out that, when the D_i is sufficiently controlled by V_{app}, a sizable frequency modulation is expected, and the frequency modulation has been enhanced with reducing the thickness of Co layer. With a 2 nm thick Co layer, the spin-wave frequency is modulated about 8% with varying the D_i from 14.7 to 0 erg/cm^2. This is one example of using collective spin wave dynamics influenced by i-DMI. The functional use of i-DMI will open up a new class of spintronic devices based on spin wave, and all-electrical structure using PSWS with a well-defined wave vector will serve as a versatile platform for such devices.

Methods. *Propagating Spin Wave Spectroscopy.* For the frequency domain measurements of spin wave propagation in the sample, a pair of antennae are connected to a vector network analyzer (model number N5222A, Keysight technologies) using GSG probes (GGB industries) and microwave coaxial cables. The frequency response of the inductive coupling is measured once with a target magnetic field and again with a reference magnetic field ($H_{ref} \sim 2000$ Oe) in which the resonance peaks are located out of the measured frequency range. Each measurement is repeated 100 times and averaged for a clear signal. The inductance matrix, which represents the inductive coupling between the antennae and ferromagnet, is calculated from the measured impedance matrix $Z_{ij}(f,H)$ as follows[23]

$$\Delta L_{ij}(f, H) = \frac{[Z_{ij}(f, H) - Z_{ij}(f, H_{ref})]}{i2\pi f}$$

■ ASSOCIATED CONTENT

Supporting Information

The Supporting Information is available free of charge on the ACS Publications website at DOI: 10.1021/acs.nanolett.5b02732.

Spin-wave excitation from meander-line antenna, the measurement of interface anisotropy, the effect of interface anisotropy on the spin wave resonance frequency, a possible frequency modulation using the electrical field control of interface anisotropy, and the finite size effect on the DMI measurements. (PDF)

■ AUTHOR INFORMATION

Corresponding Author

*E-mail: min@kist.re.kr.

Notes

The authors declare no competing financial interest.

■ ACKNOWLEDGMENTS

The authors acknowledge the technical assistance from Kun-Soo Song for the device fabrication at KIST. This work was supported by the KIST institutional program and the Pioneer Research Center Program of the National Research Foundation of Korea (NRF) grant funded by the Korea government (MSIP) (2011-0027905). K.-J.L was supported by the National Research Foundation of Korea (NRF) grant funded by the Korea government (MSIP) (NRF-2013R1A2A2A01013188, 2015M3D1A1070465).

■ REFERENCES

(1) Dzyaloshinsky, I. *J. Phys. Chem. Solids* **1958**, *4* (4), 241−255.
(2) Moriya, T. *Phys. Rev.* **1960**, *120* (1), 91−98.
(3) Bode, M.; Heide, M.; von Bergmann, K.; Ferriani, P.; Heinze, S.; Bihlmayer, G.; Kubetzka, A.; Pietzsch, O.; Blugel, S.; Wiesendanger, R. *Nature* **2007**, *447* (7141), 190−193.
(4) Yu, X. Z.; Onose, Y.; Kanazawa, N.; Park, J. H.; Han, J. H.; Matsui, Y.; Nagaosa, N.; Tokura, Y. *Nature* **2010**, *465* (7300), 901−904.
(5) Yu, X. Z.; Kanazawa, N.; Onose, Y.; Kimoto, K.; Zhang, W. Z.; Ishiwata, S.; Matsui, Y.; Tokura, Y. *Nat. Mater.* **2011**, *10* (2), 106−109.
(6) Chen, G.; Ma, T.; N'Diaye, A. T.; Kwon, H.; Won, C.; Wu, Y.; Schmid, A. K. *Nat. Commun.* **2013**, *4*, 2671.
(7) Thiaville, A.; Rohart, S.; Jué, É.; Cros, V.; Fert, A. *EPL (Europhysics Letters)* **2012**, *100* (5), 57002.
(8) Fert, A.; Cros, V.; Sampaio, J. *Nat. Nanotechnol.* **2013**, *8* (3), 152−156.
(9) Emori, S.; Bauer, U.; Ahn, S.-M.; Martinez, E.; Beach, G. S. D. *Nat. Mater.* **2013**, *12* (7), 611−616.
(10) Ryu, K.-S.; Thomas, L.; Yang, S.-H.; Parkin, S. *Nat. Nanotechnol.* **2013**, *8* (7), 527−533.

DOI: 10.1021/acs.nanolett.5b02732
Nano Lett. 2016, 16, 62−67

(11) Je, S.-G.; Kim, D.-H.; Yoo, S.-C.; Min, B.-C.; Lee, K.-J.; Choe, S.-B. *Phys. Rev. B: Condens. Matter Mater. Phys.* **2013**, *88* (21), 214401.
(12) Hrabec, A.; Porter, N. A.; Wells, A.; Benitez, M. J.; Burnell, G.; McVitie, S.; McGrouther, D.; Moore, T. A.; Marrows, C. H. *Phys. Rev. B: Condens. Matter Mater. Phys.* **2014**, *90* (2), 020402.
(13) Hiramatsu, R.; Kim, K.-J.; Nakatani, Y.; Moriyama, T.; Ono, T. *Jpn. J. Appl. Phys.* **2014**, *53* (10), 108001.
(14) Udvardi, L.; Szunyogh, L. *Phys. Rev. Lett.* **2009**, *102* (20), 207204.
(15) Zakeri, K.; Zhang, Y.; Prokop, J.; Chuang, T. H.; Sakr, N.; Tang, W. X.; Kirschner, J. *Phys. Rev. Lett.* **2010**, *104* (13), 137203.
(16) Cortés-Ortuño, D.; Landeros, P. *J. Phys.: Condens. Matter* **2013**, *25* (15), 156001.
(17) Moon, J.-H.; Seo, S.-M.; Lee, K.-J.; Kim, K.-W.; Ryu, J.; Lee, H.-W.; McMichael, R. D.; Stiles, M. D. *Phys. Rev. B: Condens. Matter Mater. Phys.* **2013**, *88* (18), 184404.
(18) Di, K.; Zhang, V. L.; Lim, H. S.; Ng, S. C.; Kuok, M. H.; Yu, J.; Yoon, J.; Qiu, X.; Yang, H. *Phys. Rev. Lett.* **2015**, *114* (4), 047201.
(19) Nembach, H. T.; Shaw, J. M.; Weiler, M.; Jué, E.; Silva, T. J. *Nat. Phys.* **2015**, *11*, 825.
(20) Stashkevich, A. A.; Belmeguenai, M.; Roussigné, Y.; Cherif, S. M.; Kostylev, M.; Gabor, M.; Lacour, D.; Tiusan, C.; Hehn, M. *Phys. Rev. B: Condens. Matter Mater. Phys.* **2015**, *91* (21), 214409.
(21) Belmeguenai, M.; Adam, J.-P.; Roussigné, Y.; Eimer, S.; Devolder, T.; Kim, J.-V.; Cherif, S. M.; Stashkevich, A.; Thiaville, A. *Phys. Rev. B: Condens. Matter Mater. Phys.* **2015**, *91* (18), 180405.
(22) Cho, J.; Kim, N.-H.; Lee, S.; Kim, J.-S.; Lavrijsen, R.; Solignac, A.; Yin, Y.; Han, D.-S.; van Hoof, N. J. J.; Swagten, H. J. M.; Koopmans, B.; You, C.-Y. *Nat. Commun.* **2015**, *6*, 7635.
(23) Vlaminck, V.; Bailleul, M. *Science* **2008**, *322* (5900), 410−413.
(24) Damon, R. W.; Eshbach, J. R. *J. Phys. Chem. Solids* **1961**, *19* (3−4), 308−320.
(25) Kalinikos, B. A.; Slavin, A. N. *J. Phys. C: Solid State Phys.* **1986**, *19* (35), 7013.
(26) Vlaminck, V.; Bailleul, M. *Phys. Rev. B: Condens. Matter Mater. Phys.* **2010**, *81* (1), 014425.
(27) Kostylev, M. *J. Appl. Phys.* **2014**, *115* (23), 233902.
(28) Khalili Amiri, P.; Rejaei, B.; Vroubel, M.; Zhuang, Y. *Appl. Phys. Lett.* **2007**, *91* (6), 062502.
(29) Schneider, T.; Serga, A. A.; Neumann, T.; Hillebrands, B.; Kostylev, M. P. *Phys. Rev. B: Condens. Matter Mater. Phys.* **2008**, *77* (21), 214411.
(30) Demidov, V. E.; Kostylev, M. P.; Rott, K.; Krzysteczko, P.; Reiss, G.; Demokritov, S. O. *Appl. Phys. Lett.* **2009**, *95* (11), 112509.
(31) Sekiguchi, K.; Yamada, K.; Seo, S. M.; Lee, K. J.; Chiba, D.; Kobayashi, K.; Ono, T. *Appl. Phys. Lett.* **2010**, *97* (2), 022508.
(32) Jamali, M.; Kwon, J. H.; Seo, S.-M.; Lee, K.-J.; Yang, H. *Sci. Rep.* **2013**, *3*, 3160.
(33) Farle, M.; Baberschke, K.; Stetter, U.; Aspelmeier, A.; Gerhardter, F. *Phys. Rev. B: Condens. Matter Mater. Phys.* **1993**, *47* (17), 11571.
(34) Oh, J. H.; Lee, K. J.; Lee, H.-W.; Shin, M. *J. Phys.: Condens. Matter* **2014**, *26* (19), 196005.
(35) Yang, H.; Thiaville, A.; Rohart, S.; Fert, A.; Chshiev, M. arXiv:1501.05511 [cond-mat.mtrl-sci].
(36) Chumak, A. V.; Serga, A. A.; Hillebrands, B. *Nat. Commun.* **2014**, *5*, 4700.
(37) Nawaoka, K.; Miwa, S.; Shiota, Y.; Mizuochi, N.; Suzuki, Y. *Appl. Phys. Express* **2015**, *8* (6), 063004.
(38) Chumak, A. V.; Vasyuchka, V. I.; Serga, A. A.; Hillebrands, B. *Nat. Phys.* **2015**, *11* (6), 453−461.
(39) Yamasaki, Y.; Sagayama, H.; Goto, T.; Matsuura, M.; Hirota, K.; Arima, T.; Tokura, Y. *Phys. Rev. Lett.* **2007**, *98* (14), 147204.

DOI: 10.1021/acs.nanolett.5b02732
Nano Lett. 2016, 16, 62−67